Vol.4, No.4, Page 1924- 1937, 2026 https://doi.org/10.59628/jast.v4i4.2602 ISSN 2958-9568 JAST

SUN PUBLISHER

مجلة جامعة صنعاء للعلوم التطبيقية والتكنولوجيا

Sana'a University Journal of Applied Sciences and Technology

https://journals.su.edu.ye/index.php/jast/

3D Static Geological Model and Volumetric Assessment of the Upper Qishn Clastic in Al Roidhat Field, Yemen

Saddam AL-Sofi [1]*, Mohammed Hail Hakimi[2], Adel Mohammad Al-Matary[3] and Bassim S. Al khirbash[1]

[1]**Department of Earth Sciences, Faculty of Petroleum and Natural Resources, Sana'a University, Sana'a, Yemen,**
[2]**Department of Geology, Faculty of Applied Science, Taiz University, 6803 Taiz, Yemen,**
[3]**Department of Petroleum Engineering, Faculty of Petroleum and Natural Resources, Sana'a University, Sana'a, Yemen**

*Corresponding author: ibnalhakimi@yahoo.com

Abstract

This study addresses a critical knowledge gap by presenting the first comprehensive 3D static geological model of the heavy-oil-bearing Upper Qishn Clastic Member in the Al Roidhat Field, Yemen. The model integrates data from eight wells. The workflow encompassed structural modeling, stratigraphic zonation into three reservoir units (S1, S2, S3), facies modeling using Sequential Indicator Simulation (30 realizations), and petrophysical property modeling using Sequential Gaussian Simulation. Probabilistic volumetric assessment was based on 100 stochastic realizations. Uncertainty analysis yields a P50 Stock-Tank Oil Initially in Place (STOIIP) of 56.81 million barrels (P10–P90 range: 44.40–73.39 MMSTB). The S3 unit exhibits the best reservoir quality (62.8% sand, 0.15 porosity, 47mD permeability), while the S1 unit shows good quality (48.1% sand, 0.14 porosity, 60 mD permeability). Yet, the S1 unit contains 58% of the STOIIP because it lies entirely within the oil column, whereas a significant portion of S3 is submerged below the oil-water contact. Together, S1 and S3 account for approximately 85% of the total resource. This pioneering 3D model quantifies reservoir heterogeneity and structural controls, establishing an essential digital foundation for the field. It demonstrates that structural position can override intrinsic rock quality in governing hydrocarbon distribution, and it clearly identifies the S1 and S3 units as priority targets for future development and enhanced oil-recovery planning in this challenging heavy-oil reservoir.

Article Info

Keywords:
3D Geological Model, Heavy Oil, Upper Qishn Clastic, Uncertainty Analysis, Reservoir Characterization, Al Roidhat Field, STOIIP.

Article History:
Received: 8-December-2025,
Revised: 7-March-2026,
Accepted: 2-April-2026,
Published: 28 April 2026.

1. INTRODUCTION

1.1. Regional Context and Research Focus

The Sayun-Masila Basin in eastern Yemen (Fig. 1) is a prolific hydrocarbon province in the East African Rift System [1]. Within Block 9, the Al Roidhat Field presents a distinctive development challenge owing to its heavy-oil accumulation, which is in notable contrast to the lighter crudes produced from neighboring structures such as Hiswah and Auqban [2, 3]. This study targets the field's primary reservoir, the Cretaceous Upper Qishn Clastic Member, aiming to transform its characterization using advanced three-dimensional modeling.

1.2. The Defined Knowledge Gap and Problem Statement

Despite the economic potential of this resource, a critical scientific and technical gap persists, namely, the absence of peer-reviewed research and a high-resolution 3D static geological model for this reservoir. The current understanding and field development criteria rely on internal operator reports and 2D correlations [3]. These approaches are fundamentally inadequate for quantify-

ing the spatial heterogeneity and volumetric uncertainty inherent to the complex depositional system of the Upper Qishn Clastic Member, leading to significant risks in development planning.

1.3. Methodological Framework: Addressing Heterogeneity and Uncertainty

To bridge this gap, we implemented an integrated geostatistical reservoir modeling workflow, which is recognized as the standard for quantifying subsurface complexity [4, 5]. This probabilistic approach was specifically designed to move beyond deterministic interpretations. The workflow progresses from structural framework construction to volumetric assessment, employing Sequential Indicator Simulation (SIS) to model lithofacies architecture and Sequential Gaussian Simulation (SGS) to populate the model with petrophysical properties [6–8]. By generating multiple realizations, this framework facilitates probabilistic volumetric assessment (P10, P50, P90), explicitly quantifying uncertainty for risk-informed decision-making [9, 10].

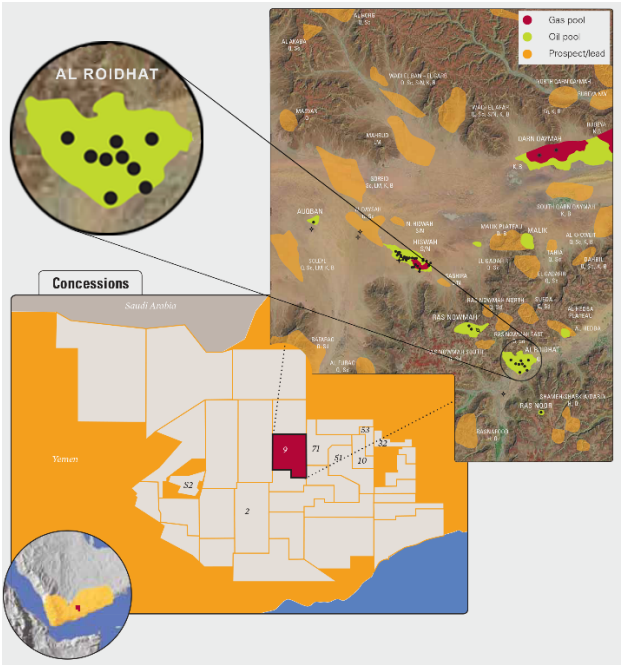

Figure 1. Location map of Block 9 in the Sayun- Masila Basin, Yemen, showing the Al Roidhat Field (study area).

1.4. Research Objectives and Novel Contribution

This study was designed to deliver the first comprehensive 3D static geological model and the inaugural peer-reviewed study of the Upper Qishn Clastic Member in the Al Roidhat Field. The specific objectives are as follows:

1. Construct an integrated structural and stratigraphic framework utilizing data from eight wells.
2. Model the three-dimensional distribution of lithofacies and key petrophysical properties (effective porosity, permeability, and water saturation) using SIS and SGS.
3. Evaluate the governing influence of depositional facies heterogeneity on reservoir architecture and connectivity.
4. Provided a probabilistically robust estimate of Stock Tank Oil Initially in Place (STOIIP), quantifying resource uncertainty through P10, P50, and P90 scenarios.

The fulfillment of these objectives will produce a quantitatively rigorous digital asset, establishing an essential foundation for this field by resolving key subsurface uncertainty.

2. GEOLOGICAL SETTING

2.1. Basin Framework and Tectonic Evolution

The Al Roidhat Field is situated within Block 9 of the Sayun-Masila Basin (Fig. 1), an asymmetric extensional basin formed during the Late Jurassic to Early Cretaceous rifting associated with the breakup of Gondwana [1, 2]. The present-day architecture of the basin, dominated by NW-SE trending half-grabens bounded by major normal faults, has fundamentally controlled sediment distribution and created structural traps within the basin [1, 11].

2.2. Reservoir and Seal Stratigraphy

The primary reservoir target is the Upper Qishn Clastic Member of the Cretaceous Qishn Formation (Fig. 2). Analysis of the core and log data from the field defines this member as a heterogeneous succession of fine- to medium-grained sandstones interbedded with shaly sandstone and shale. This lithological assemblage is diagnostic of deposition in a fluvial-deltaic to shallow-marine environment, which is the principal control on the inherent spatial variability and compartmentalization of the reservoir [2, 3, 11].

An effective, multi-layer seal system is critical to the petroleum system in the field. The Qishn Carbonate Member directly overlies the clastic reservoir, providing an immediate top seal. The Harshiyat Formation, a regionally extensive unit composed predominantly of shale and marl, forms the ultimate regional top seal, ensuring hydrocarbon entrapment [1, 12].

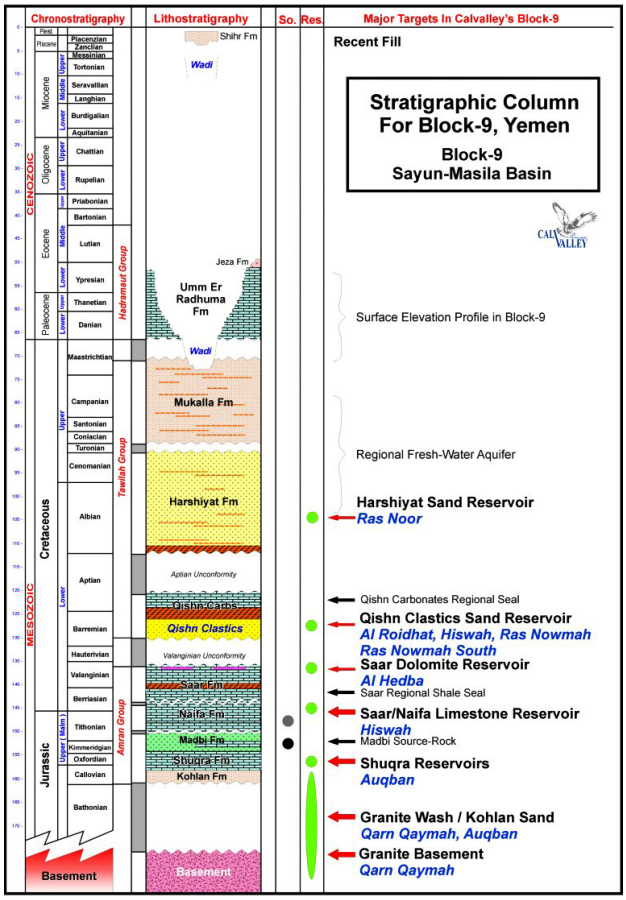

Figure 2. Generalized stratigraphic column of Block 9, illustrating the vertical succession and the position of the Upper Qishn Clastic Member.

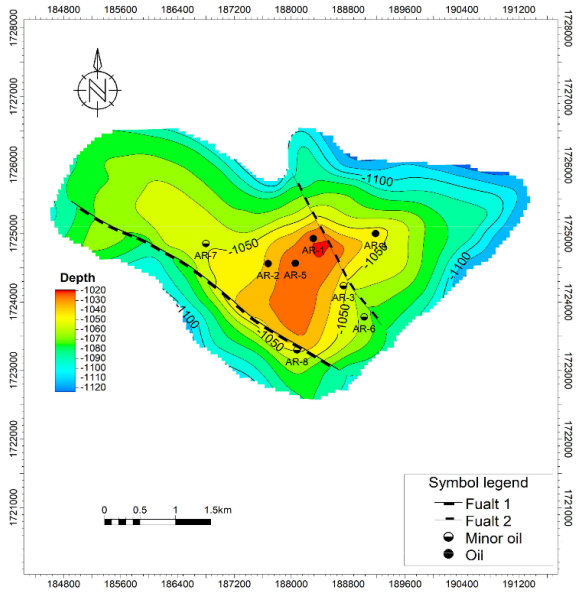

Figure 3. Structural map (Top Upper Qishn Clastic Member) of the Al Roidhat Field, showing the gentle anticlinal structure and fault traces.

2.3. Structural Configuration of the Al Roidhat Field

Structurally, the field forms a gentle, broad NW-SE-trending anticline, consistent with the regional tectonic grain. The main structural complexities within the reservoir interval are a set of minor, NW-SE-trending normal faults (Fig. 3). Interpretations from well tops and seismic-derived maps indicate that these faults have minimal throws (typically <5 m) [3]. Therefore, they are interpreted as non-sealing and are not considered significant barriers to lateral fluid flow at the reservoir scale; their primary influence is limited to creating subtle offsets that may affect local variations in the formation thickness.

3. MATERIALS AND METHODS

3.1. Data Sources and Quality Control

This study integrated a comprehensive dataset from the Al Roidhat Field, Block 9, Sayun-Masila Basin, Yemen. The dataset comprises:

- Well Logs: Digital logs from eight wells, including Gamma Ray (GR), density (RHOB), neutron (NPHI), sonic (DT), and resistivity (LLD, LLS).
- Geological Data: Core descriptions and interpreted stratigraphic markers.
- Structural Data: Horizon and fault polygons digitized from structural maps and well tops.

All well logs were depth-matched to a common datum and subjected to a standardized quality control (QC) workflow. This process involved identifying and correcting acquisition artifacts, such as spikes, null values, and borehole washouts, using caliper logs. Gamma Ray logs were normalized across the field to ensure consistency in lithology interpretation [5, 13].

3.2. Petrophysical Analysis and Cut-off Definition

Petrophysical interpretation was performed using Interactive Petrophysics (IP v3.5) software [14]. Effective porosity (PHIE) was calculated from density-neutron cross-plots, with calibration of the core data where available. Water saturation (Sw) was estimated using the Archie equation with locally tuned parameters (m, n, Rw).

Critical net-pay and facies cutoffs were adopted directly from the operator's internal field report (Callvalley Petroleum Co., 2007) [3], ensuring alignment with the established field development criteria. The applied cutoffs were as follows:

- Clay Volume (Vclay): ≤ 0.30
- Effective Porosity (PHIE): ≥ 0.08
- Water Saturation (Sw): ≤ 0.65

These cutoffs were used sequentially to define the net

reservoir (Vclay $\leq$ 0.30 and PHIE $\geq$ 0.08) and pay zones (Sw $\leq$ 0.65). The Vclay cutoff of 0.30 also served as the primary discriminator between Sand (Vclay < 0.30) and Shaly Sand (Vclay $\geq$ 0.30) facies, which is a standard practice in heterogeneous clastic reservoirs [4, 6]. The interpreted logs were subsequently upscaled to a 3D simulation grid resolution (Figure 4).

3.3. Stratigraphic Zonation and Layering

A high-resolution stratigraphic framework was established through detailed well-to-well correlation, utilizing GR and Sonic log signatures alongside core descriptions. This allowed the subdivision of the Upper Qishn Clastic Member into three principal reservoir units (S1, S2, and S3), representing a transgressive-regressive sequence. To accurately capture the impact of thin, laterally continuous shale layers on vertical connectivity, each unit was subdivided into five layers, resulting in a total of 15 layers within the model. This detailed layering is essential for representing fine-scale heterogeneity in three-dimensional (3D) static models [15, 16].

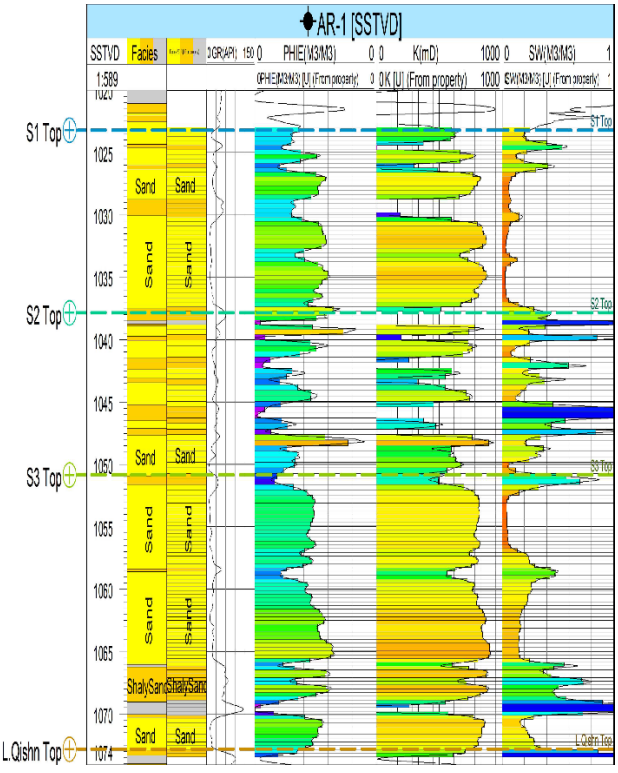

Figure 4. Upscaled petrophysical logs (facies, porosity, water saturation, permeability) for Well AR-1.

3.4. Structural Modeling and Grid Construction

Structural modeling was conducted using Schlumberger Petrel™ (v2009). Key horizons, including the top and base of the reservoir and two NW–SE-trending normal faults, were interpreted from well tops and structural maps. These faults were modeled as non-sealing elements because of their minimal throws (<5 m), consistent with field studies [13].

A 3D corner-point grid with lateral cell dimensions of 300 m × 200 m was constructed for the model. This grid resolution was specifically chosen to ensure an accurate representation of the thin reservoir layers and clay interbeds, as well as the key spatial heterogeneities of the reservoir. This allows the preservation of spatial correlation for petrophysical properties (porosity, permeability, and facies) and alignment with average well spacing.

The vertical grid resolution was selected to capture layer thickness variations and minor fault offsets, ensuring that both the stratigraphic and structural complexities of the Upper Qishn Clastic are accurately represented.

The grid quality was rigorously validated. The resulting metrics (Table 1) confirm the grid's geometric integrity: cell angles reach a maximum of 90° only locally near faults, which is an expected and acceptable condition in faulted zones, while the overall grid remains conformal with a mean cell angle of 5.05°. Inside-out cells were minimal (>0 only near faults), and all cell volumes were positive. A 3D visualization of the quality-checked grid is presented in Figure 5.

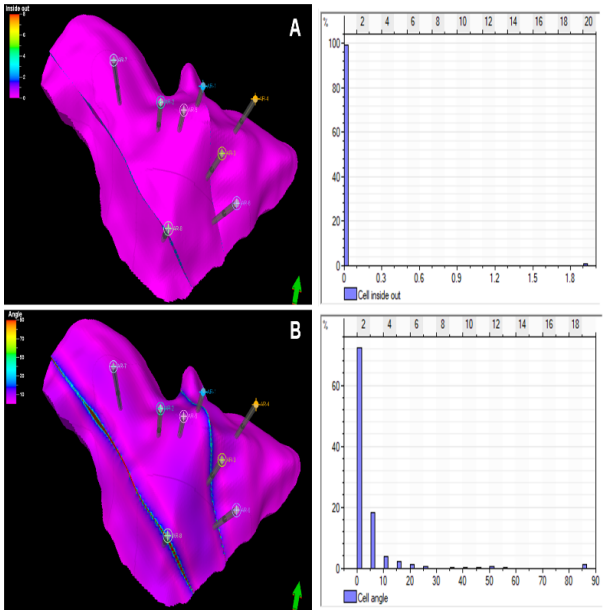

Figure 5. Structural grid quality control: (A) cell angle distribution, (B) inside-out cells.

Table 1. Structural grid quality control metrics.

Parameter	Min	Max	Mean	Std	Comment
Cell Angle	0	90	5.05	10.4	High values occur locally near faults, overall grid is conformal
Cell Inside Out	0	2	0.01	0.14	>0 only near faults
Cell Volume	positive				All volumes are positive (pass)

3.5. Facies Modeling and Uncertainty Quantification

Lithofacies at the well locations were classified into Sand, Shaly Sand, and Shale. Their 3D spatial distribution was modeled using Sequential Indicator Simulation (SIS), a geostatistical method specifically designed for categorical data that honors facies proportions and spatial continuity observed in wells [17–21]. The experimental indicator variograms were calculated and modeled for each facies within each reservoir unit (Table 2, Figure 6). Given the limited number of wells (eight), which restricts the statistical robustness of directional variogram analysis, the variogram models were primarily guided by the vertical variability of the well data and geological understanding of depositional environment trends (e.g., longer continuity along the NW-SE depositional axis). This approach is a recognized practice in fields with sparse well control [9, 15].

Table 2. Indicator variogram parameters for the Sand, Shaly Sand, and Shale lithofacies in each reservoir unit.

Lithofacies	Major	Minor	Vertical	Sill	Nugget	Azimuth	Variogram Type
	Range			Variogram Parameter			
Sand	1000	500	3	0.99	0.3	135	Spherical
Shaly Sand	508	300	2	0.949	0.159	135	Spherical
Shale	623	400	2.2	0.91	0.09	135	Spherical
Sand	890	300	2	0.82	0.32	135	Spherical
Shaly Sand	400	200	1.6	0.99	0.58	135	Spherical
Shale	522	300	2.6	0.92	0.32	135	Spherical
Sand	615	442	2.1	0.98	0.37	135	Spherical
Shaly Sand	488	200	1.6	0.93	0.36	135	Spherical
Shale	564	300	1.8	0.78	0.07	135	Spherical

Thirty equiprobable realizations were generated to quantify the uncertainty inherent in the facies distribution, 30 equiprobable realizations were generated. From this ensemble, the realization that provided the best overall match to the well data (facies [22]) was selected as the base case for property modeling. This selection was based on the quantitative minimization of the Mean Square Error (MSE) between the simulated and actual facies proportions at all well locations (Table 3).

Table 3. Comparison of base, high, and low case facies realizations based on Mean Square Error (MSE) match with well data

Status	Realization	MSE vs. well	Key match
Base case	Facies [23]	1.763	Best overall
High case	Facies [18]	1.546	Best in S1 unit
low case	Facies [3]	2.323	Conservation bias in S2

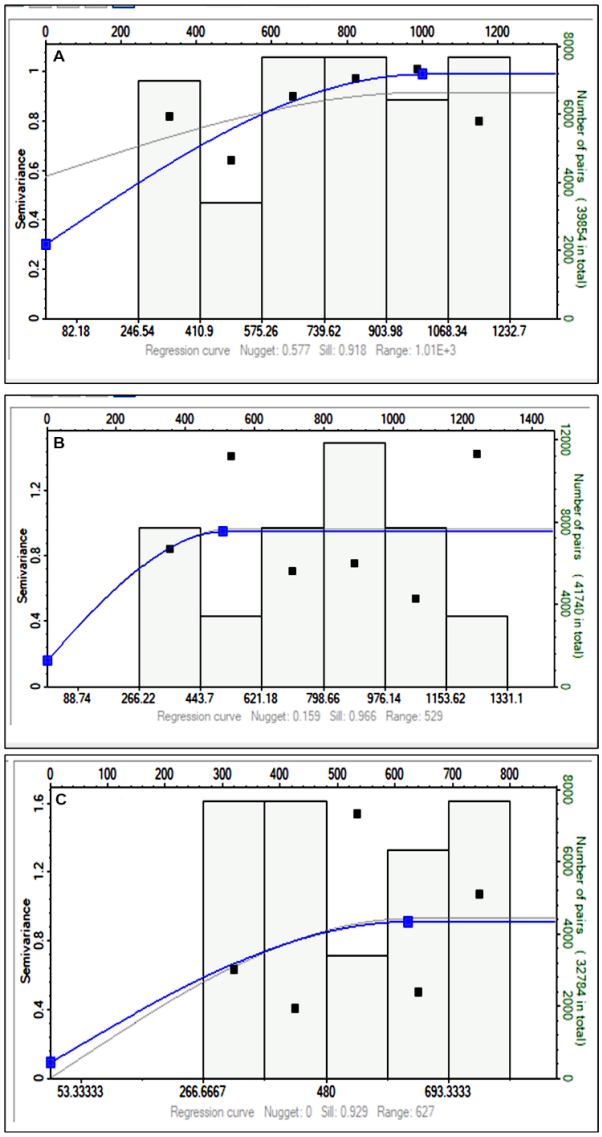

Figure 6. Experimental and fitted indicator variograms for the Sand, Shaly Sand, and Shale lithofacies.

3.6. Petrophysical Property Modeling and Validation

Continuous petrophysical properties, such as effective porosity (PHIE), permeability (K), and water saturation (Sw), were modeled within each facies type using Sequential Gaussian Simulation (SGS) [8, 19, 23]. The simulation was constrained by the base-case facies model and directly conditioned to upscaled well log data. Separate variogram models were defined for each property within the dominant "Sand" facies.

Rigorous property-specific quality control (QC) was performed. This included comparing the statistical distributions (mean, variance, and histogram shape) and spatial trends of the simulated properties with the input well data. Quantitative metrics, such as the average absolute error and correlation coefficient between the simulated and actual log values at the wells, were evaluated. The model's ability to reproduce geologically realistic relation-

ships (e.g., porosity-permeability transformations) was also verified. Visual and statistical validation was demonstrated through cross-sectional and well-log comparisons (Figures 13, 15, 17, and 19).

3.7. Volumetric Estimation and Uncertainty Analysis

A stochastic framework was employed to provide a robust probabilistic assessment of hydrocarbons in place. One hundred (100) stochastic realizations of the Stock Tank Oil Initially in Place (STOIIP) were generated by sampling from the facies (30 realizations) and property model uncertainties. For each realization, the Hydrocarbon Pore Volume (HCPV) and STOIIP were calculated per grid cell using the standard volumetric formula and summed:

$$\text{STOIIP} = 7758 \times A \times h \times \phi \times (1 - Sw) / Bo \quad (1)$$

where Bo = 1.029 RB/STB, as obtained from the PVT analysis. The results are reported as P10 (conservative), P50 (median), and P90 (optimistic) estimates for each reservoir unit and the total reservoir (Table 5), with the distribution of outcomes visualized in Figure 20 [10, 16, 22].

3.8. Workflow Integration

The complete integrated modeling workflow, encompassing data loading, petrophysical analysis, structural and stratigraphic modeling, facies and property simulation, and culminating in probabilistic volumetric calculation, is summarized schematically in Figure 7.

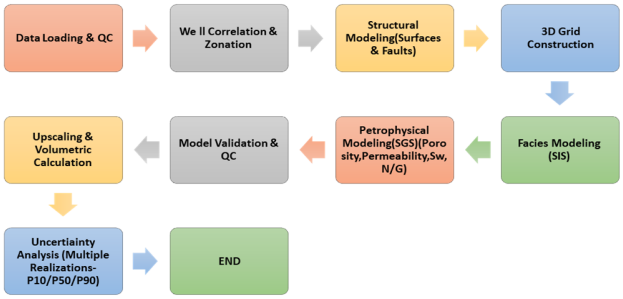

Figure 7. Integrated 3D static geological modeling workflow diagram.

4. RESULTS AND DISCUSSION

4.1. Structural Framework and Fault Impact

The 3D structural model (Fig. 8), constructed following the methodology in Section 3.4, confirms that the field is a gentle NW-SE-trending anticline.

The two interpreted normal faults had throws <5 m, consistent with the seismic-derived maps used as input. Grid quality control metrics (Table 1) confirmed the geometric integrity of the model, with cell distortions localized only near faults (Fig. 5). The OWC map and cross-section (Fig. 9) demonstrate that the contact depth varies systematically with structural elevation (1063 to 1082 m) and is not displaced across faults. This finding, derived directly from the integrated model, confirms the initial methodological assumption (Section 3.4) that these faults are non-sealing and do not compartmentalize the reservoir, a key clarification requested by reviewers regarding structural influence.

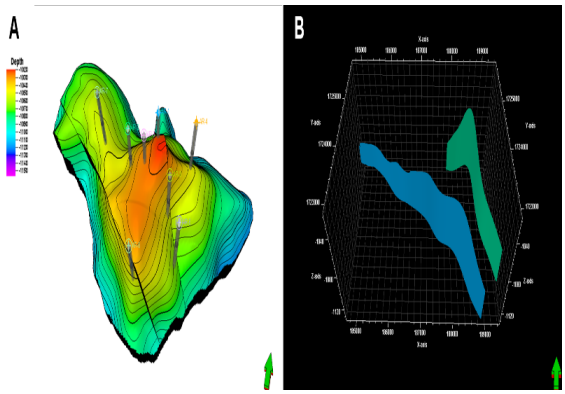

Figure 8. 3D structural and fault model of the Upper Qishn Clastic Member, visualizing the anticlinal geometry and the incorporated non-sealing faults.

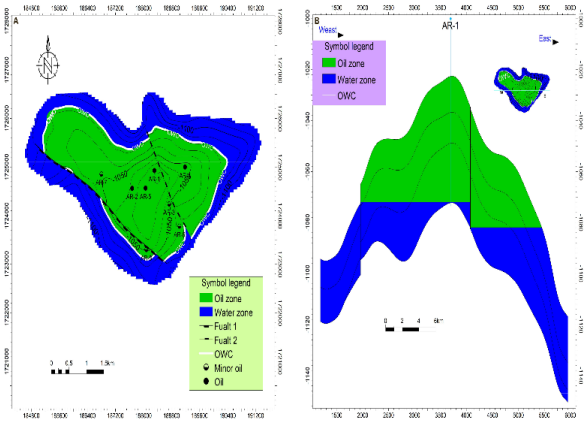

Figure 9. (A) Map view of the Oil-Water Contact (OWC) depth across the field. (B) West-east cross-section illustrating the OWC variation with structural segments.

4.2. Stratigraphic Architecture and 3D Facies Heterogeneity

The 15-layer zonation scheme (Section 3.3) enabled the detailed capture of vertical heterogeneity. The 3D

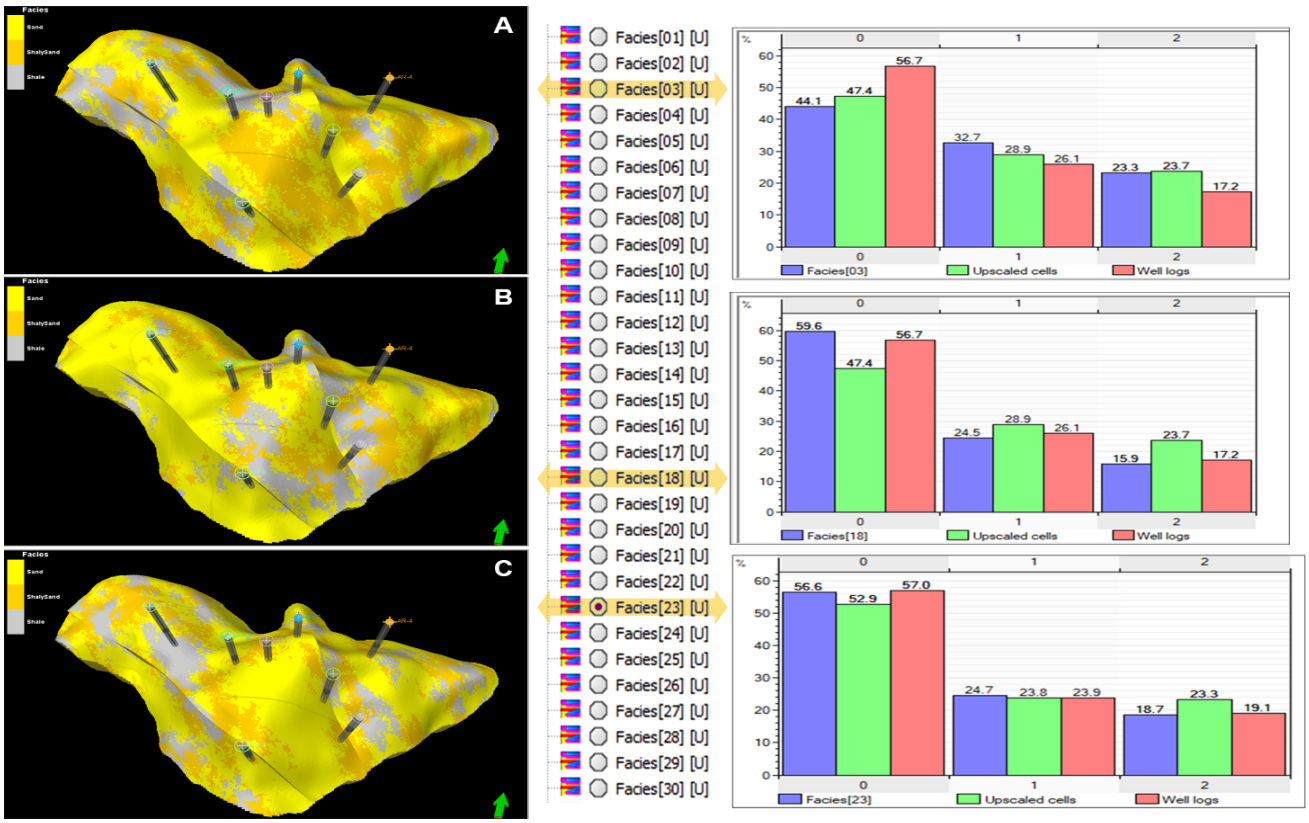

Figure 10. Three equiprobable facies realizations for the S1 reservoir unit, generated using Sequential Indicator Simulation (SIS).

facies models (Figures 10, 11, 12) show a clear contrast between the three units: the fluvial-deltaic S3 unit has the highest sand content (62.8%) and greatest thickness; the shallow marine S1 unit shows good reservoir quality with 48.1% sand; while the transitional S2 unit is more heterogeneous and shaly (42.3% Shaly Sand, 27.7% Shale).

These quantitative facies distributions obtained through Sequential Indicator Simulation (SIS) of well data (Section 3.5) characterize the reservoir's lateral and vertical heterogeneity. Subsequent volumetric analysis (Section 4.4) revealed that the S1 unit contained the largest share of hydrocarbons (58% of the STOIIP) despite S3's superior rock quality, because a significant portion of S3 lies below the oil-water contact. This vertical heterogeneity is illustrated in the cross section (Figure 13).

4.3. Petrophysical Property Models

Validation and Trends The property models for porosity, permeability, and water saturation (Figs. 14, 16, and 18) are the direct output of the Sequential Gaussian Simulation (SGS) workflow (Section 3.6). Their validation is demonstrated by the close match between the simulated properties and the upscaled well logs in cross-sections (e.g., Fig. 15, 17, and 19), addressing the reviewer's request for "quantitative validation metrics". The statistical summary (Table 4) provides a consistent, definitive set of average properties called for by reviewers to resolve earlier discrepancies. Analysis of these tabulated values demonstrates a clear trend: high porosity/permeability in S1/S3 and low in S2, which directly reflects the contrasting facies proportions between the sand-rich S1/S3 units and the shaly S2 unit. However, the subsequent volumetric analysis (Section 4.4) demonstrates that superior petrophysical properties do not always translate to volumetric dominance, as the structural position relative to the OWC plays a decisive role in determining hydrocarbon distribution.

Table 4. Statistical summary of petrophysical properties for the S1, S2, and S3 reservoir zones.

S1 zone	PHIE	SW	Kmd	N/G
Min	0	0.017	0	0
Max	0.32	1	623	0.83
Mean	0.14	0.41	60	0.543
Std	0.09	0.37	112	0.237
S2 zone	PHIE	SW	Kmd	N/G
Min	0	0.024	0	0
Max	0.3	1	443	0.77
Mean	0.08	0.55	13.7	0.417
Std	0.07	0.32	54	0.235
S3 zone	PHIE	SW	Kmd	N/G
Min	0	0.025	0	0
Max	0.31	1	539	0.77
Mean	0.15	0.40	47	0.70

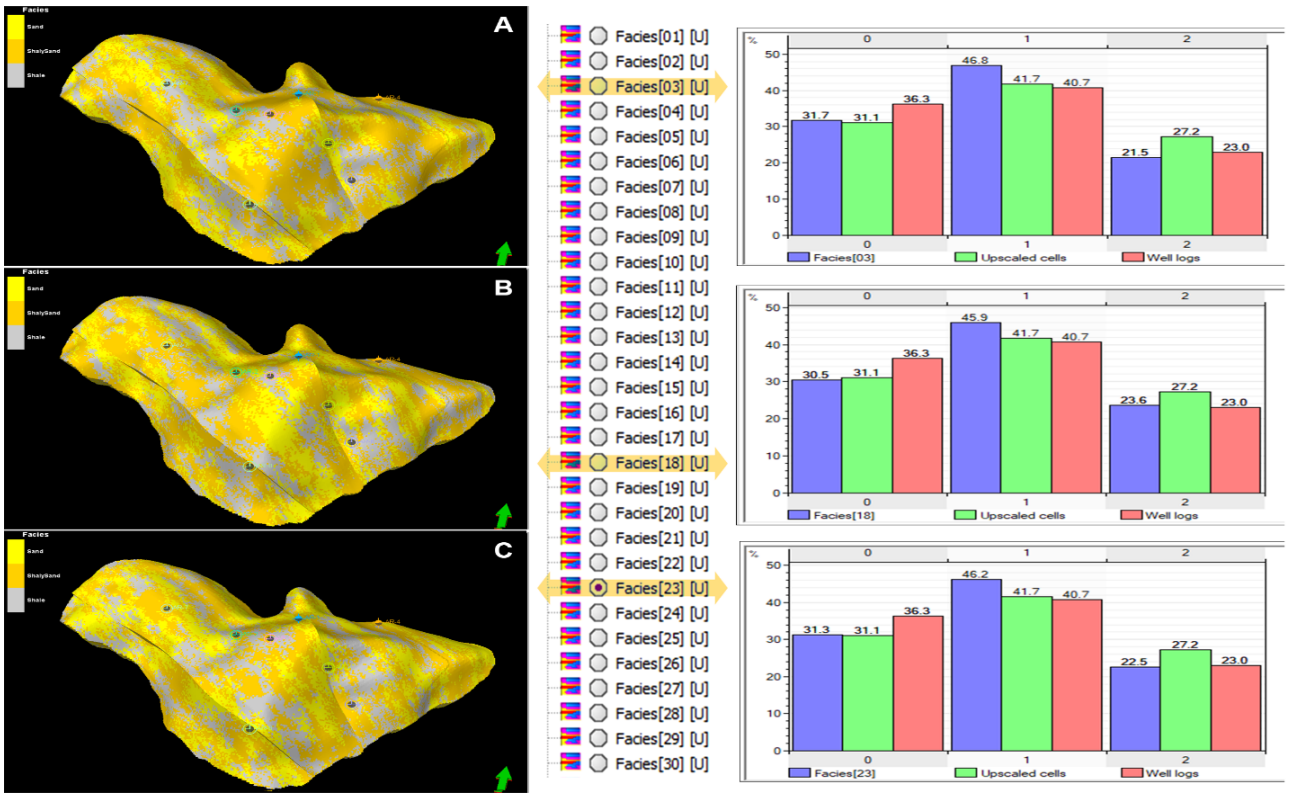

Figure 11. Three equiprobable facies realizations for the S2 reservoir unit.

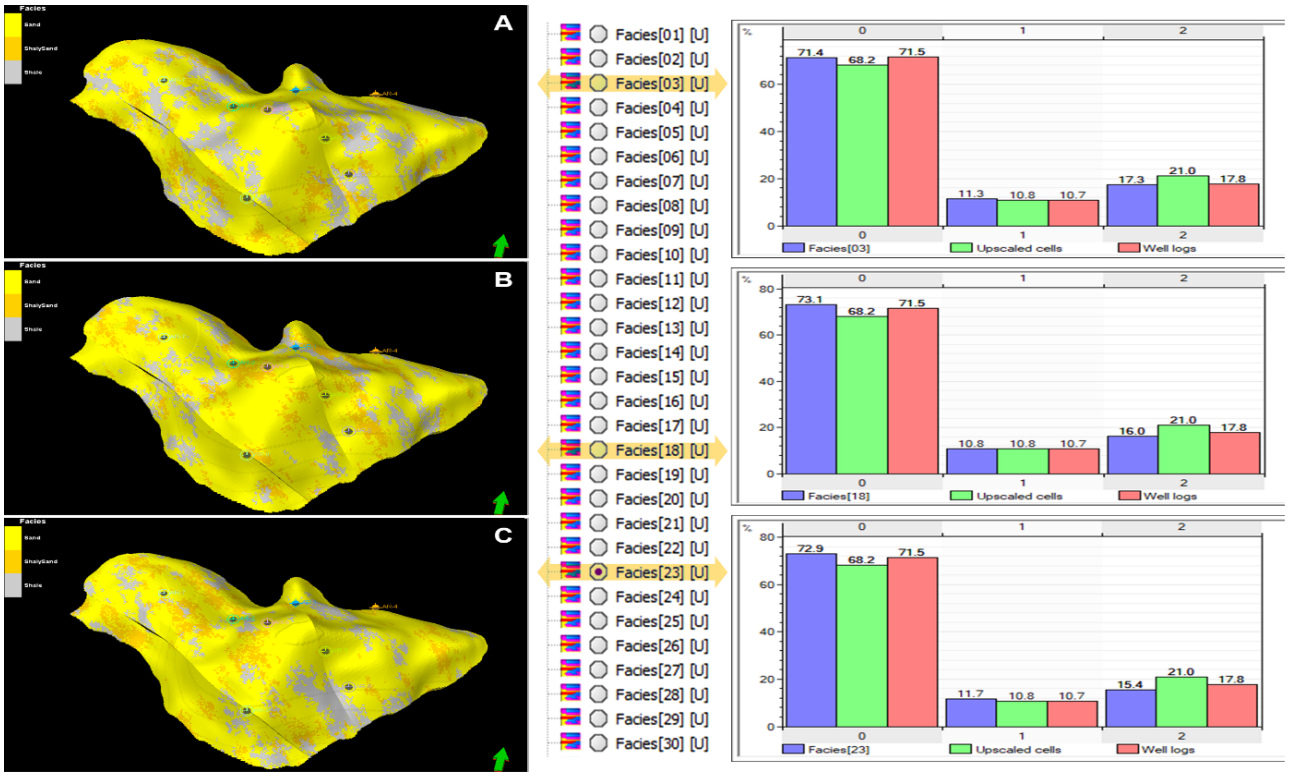

Figure 12. Three equiprobable facies realizations for the S3 reservoir unit, generated using Sequential Indicator Simulation (SIS).

This confirms that the depositional environment is the primary control on reservoir quality, while highlighting the critical influence of post-depositional structural evolution.

4.4. Probabilistic Volumetrics and Uncertainty Quantification

This section directly and fully addresses the major reviewer critique of the "missing quantitative uncertainty

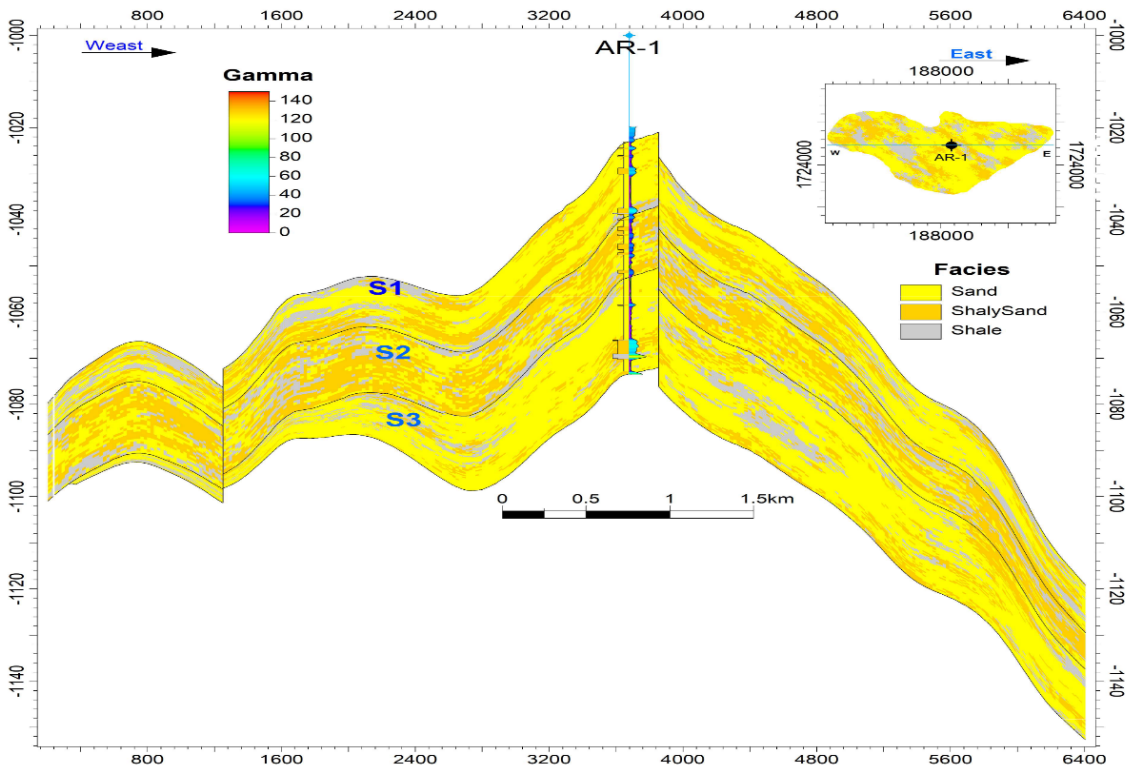

Figure 13. West-east cross-section showing the vertical facies distribution with Gamma Ray (GR) logs for quality control.

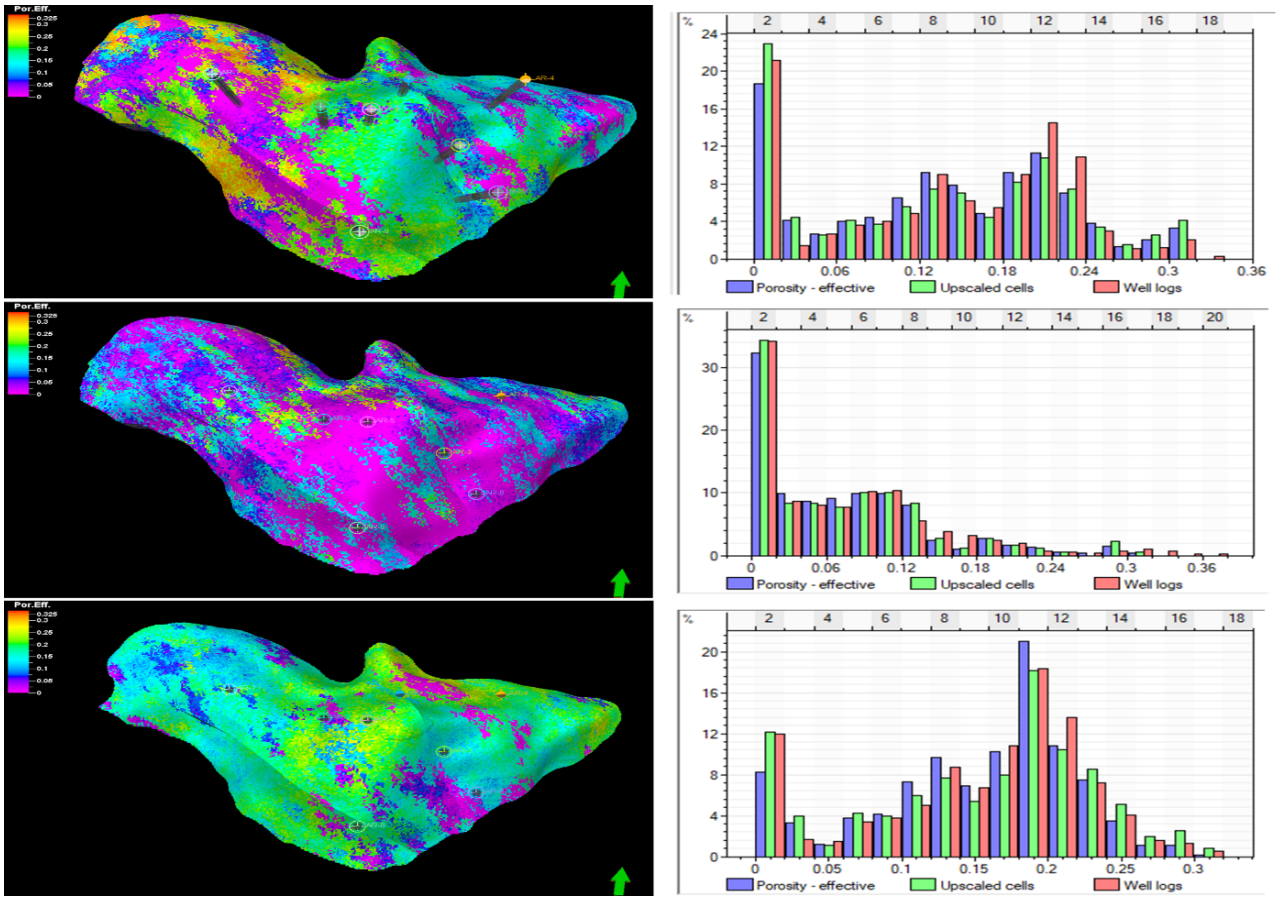

Figure 14. Final porosity (PHIE) model for the (A) S1, (B) S2, and (C) S3 units, with quality control (QC) plots.

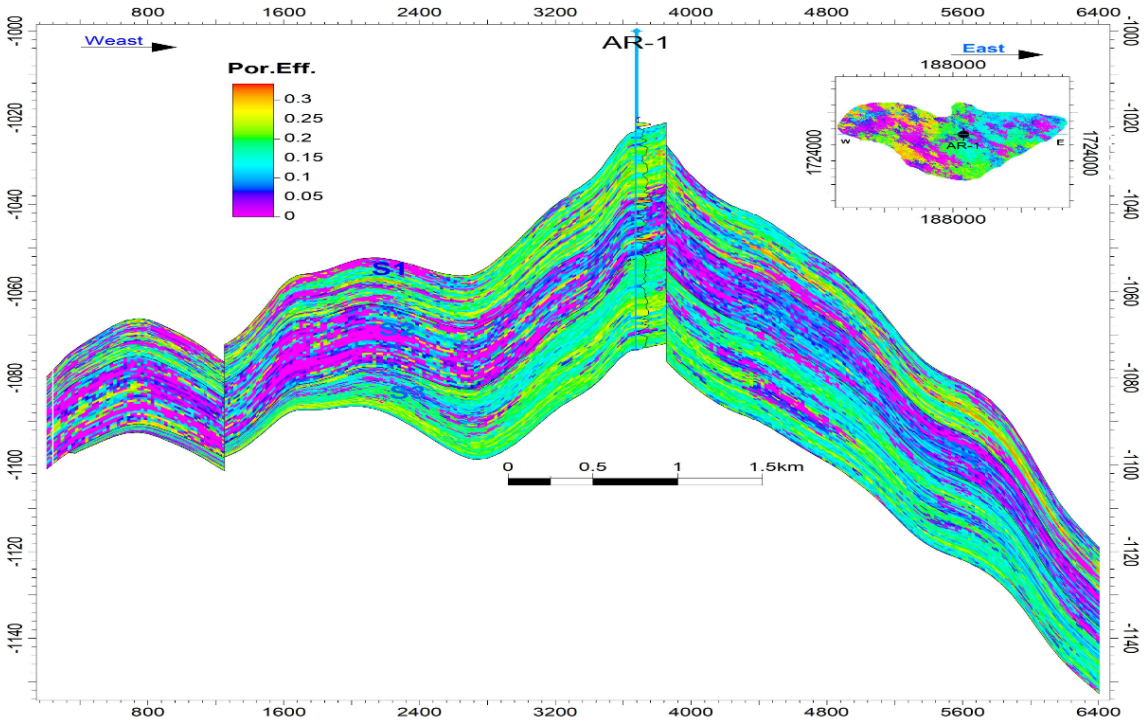

Figure 15. West-east cross-section showing the vertical porosity distribution and QC with well logs.

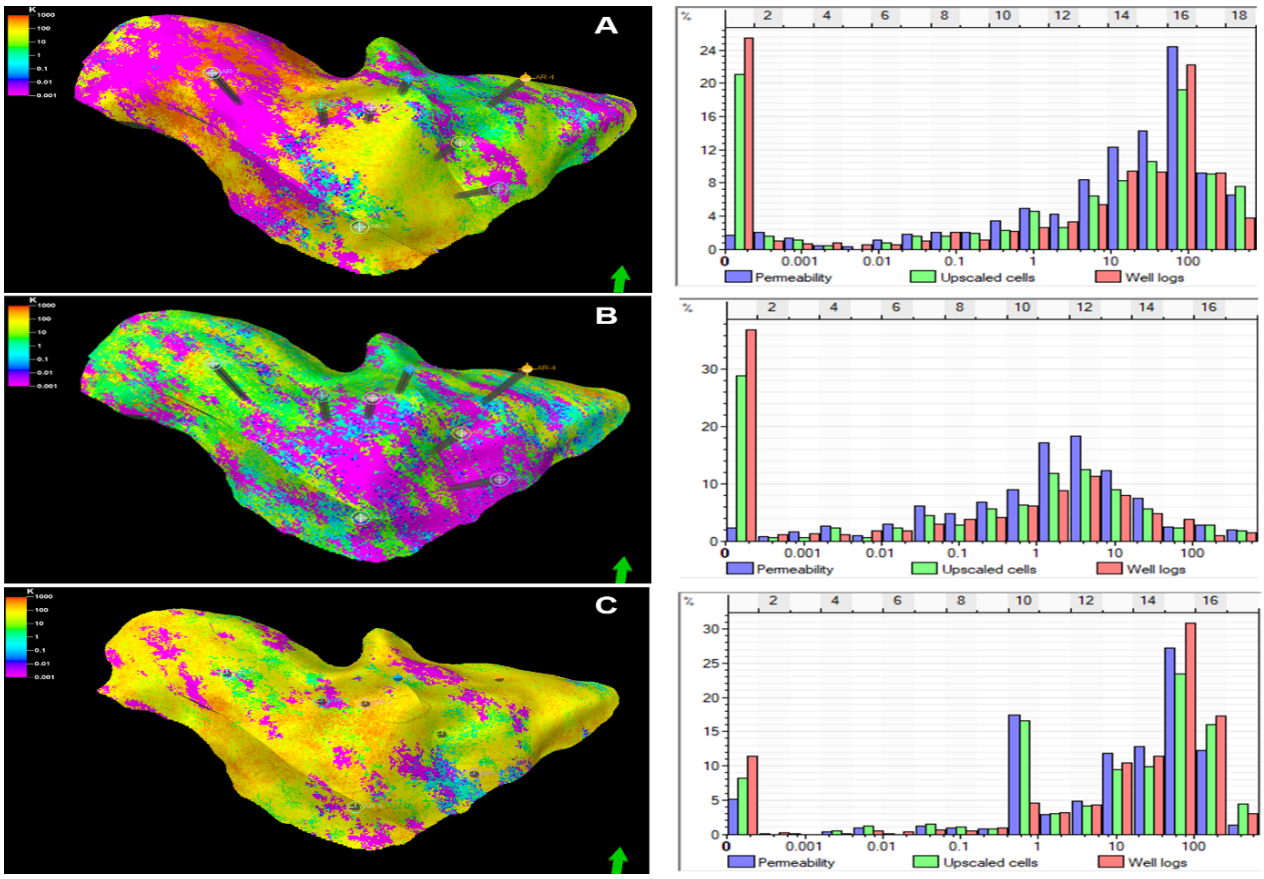

Figure 16. Final permeability (K) model for the (A) S1, (B) S2, and (C) S3 units, with QC plots.

reporting." The 100 stochastic realizations of the STOIIP (Fig. 20), generated by propagating facies and property uncertainty (methodology, Section 3.7), yielded the probabilistic results in Table 5:

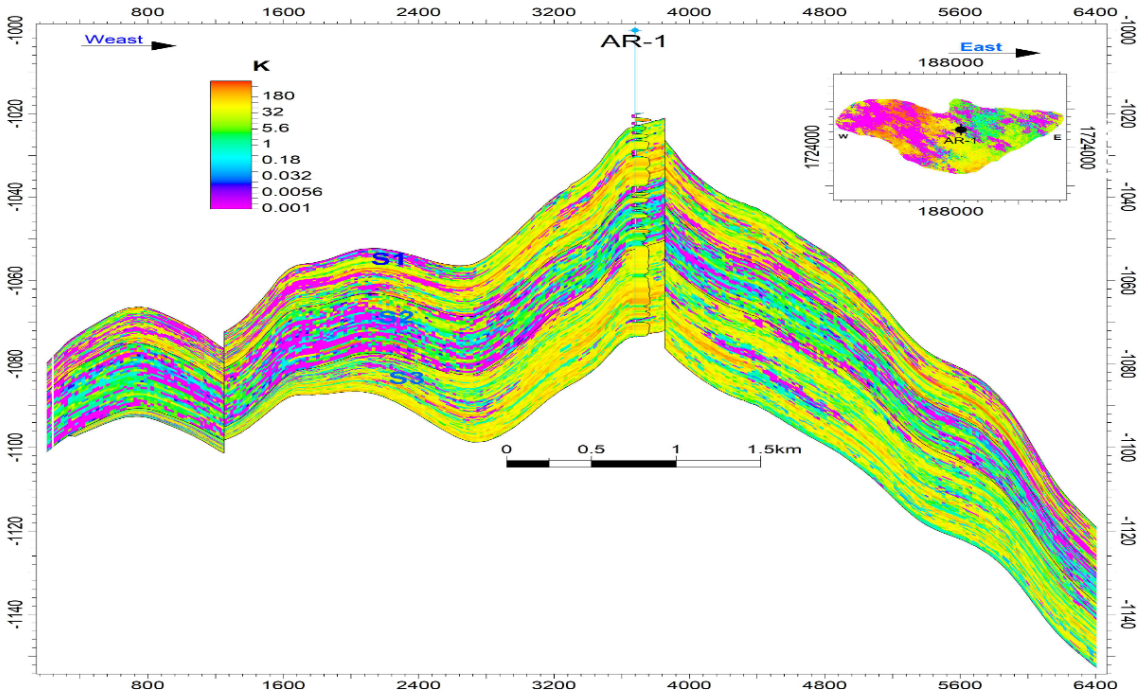

Figure 17. West-east cross-section showing the vertical permeability distribution and QC with well logs.

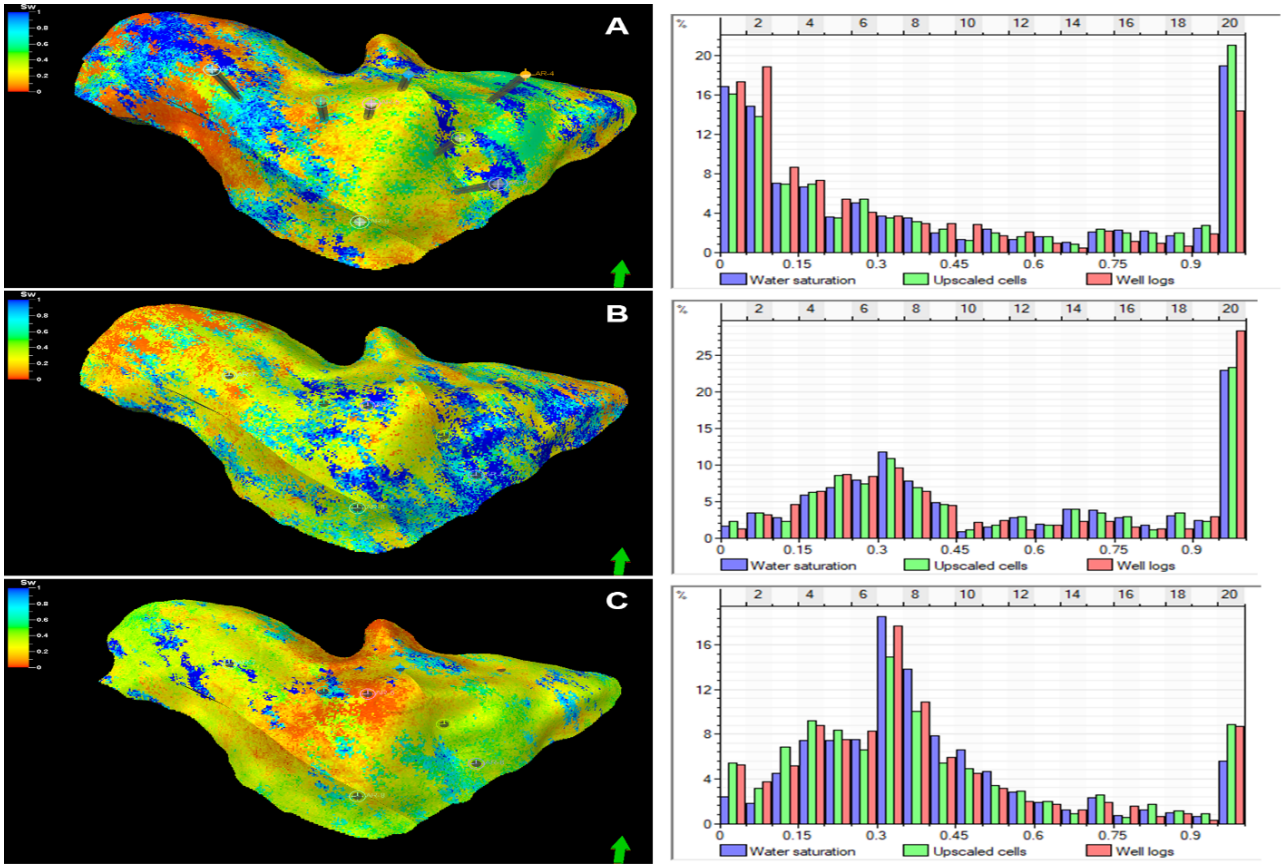

Figure 18. . Final water saturation (Sw) model for the (A) S1, (B) S2, and (C) S3 units, with quality control (QC) plots.

- Total P50 STOIIP: 56.81 MMSTB
- P10-P90 Range: 44.40 – 73.39 MMSTB (a ±29% uncertainty envelope)
- Distribution: S1 (58%), S3 (27%), and S2 (15%)

An important insight from the volumetric analysis is the

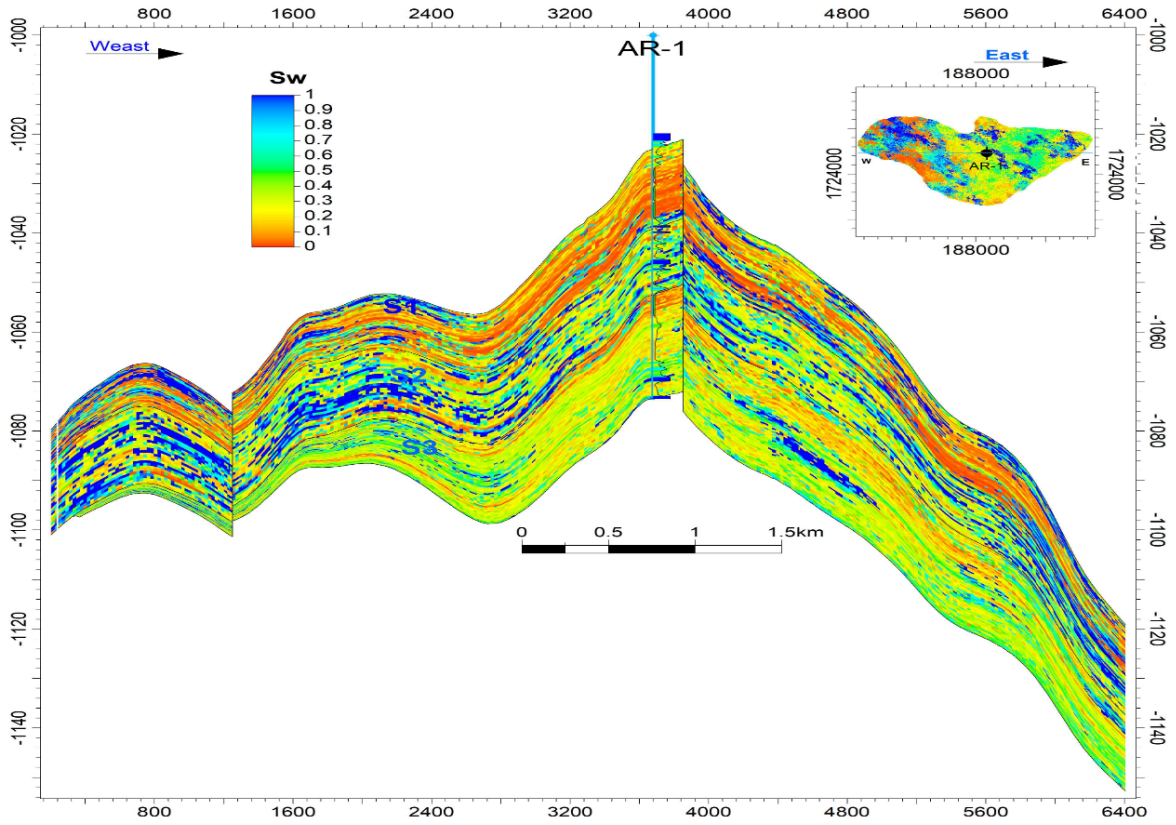

Figure 19. West-east cross-section showing the vertical water saturation distribution and QC with well logs.

dominance of the S1 unit (58% of the STOIIP) over the S3 unit (27% of the STOIIP), despite S3's superior reservoir characteristics including high sand content and greater thickness. This counterintuitive result is explained by examining the structural framework: a significant portion of the thick, high-quality S3 sands lies below the oil-water contact (Figure 9B), rendering them water-saturated. In contrast, the entire S1 unit is situated within the oil column, allowing its full rock volume to contribute to the hydrocarbon storage. This finding underscores how structural positions can override depositional facies quality in controlling hydrocarbon accumulation patterns.

Providing these P10/P50/P90 values and the uncertainty range explicitly meets the reviewer's demand and transforms the volumetric assessment from deterministic to risk-informed assessment.

4.5. Synthesis: Addressing the Research Gap and Implications

This integrated 3D model (workflow summarized in Fig. 7) successfully bridges the research gap identified in the introduction, that is, the lack of a comprehensive 3D model for the Al Roidhat Field. It moves beyond regional studies [1, 11] and 2D correlations of prior work [2, 3] by providing:

1. Quantified Heterogeneity Map: Facies and property models (Figs. 9-19) give spatial dimensions to reservoir quality.
2. A Clarified Structural Role: The model demonstrates that faults are non-sealing (Figs. 8, 9), reducing compartmentalization uncertainty.
3. A Probabilistic Resource Base: The STOIIP range (Table 5, Fig. 20) is foundational for development planning.

Table 5. Probabilistic volumetric estimation results (P10, P50, P90) for the S1, S2, S3 units and total reservoir.

Zones	Probability	BV ($*10^6 ft^3$)	PV ($*10^6\ ft^3$)	HCPV ($*10^6$RB)	STOIP (MSTB)
S1	P10	2756.35	45.67	29.23	28.41
	P50	3353.96	54.80	33.99	33.03
	P90	3935.44	63.97	40.12	38.99
S2	P10	1450.26	12.87	6.49	6.30
	P50	1867.19	17.21	8.58	8.34
	P90	2506.93	23.06	11.95	11.62
S3	P10	687.74	15.61	9.97	9.69
	P50	1084.00	24.23	15.88	15.44
	P90	1647.41	37.01	23.45	22.79
UP.Qishn Clastic	P10	4894.35	74.14	45.69	44.40
	P50	6305.15	96.24	58.46	56.81
	P90	8089.78	124.03	75.52	73.39

The model conclusively identified the S1 and S3 units as high-quality, high-potential targets. Notably, S1 con-

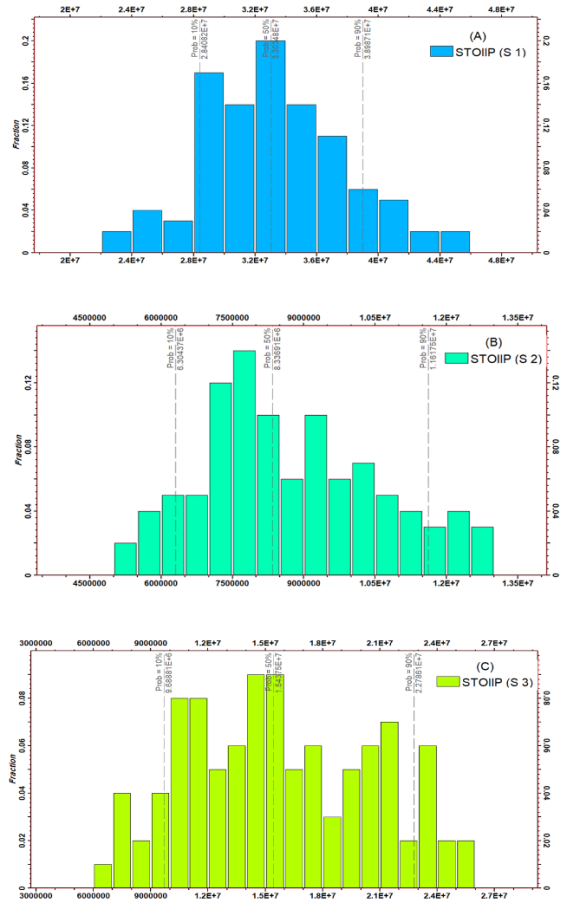

Figure 20. Distribution of 100 stochastic realizations of Stock Tank Oil Initially in Place (STOIIP) for the (A) S1, (B) S2, and (C) S3 reservoir units, illustrating volumetric uncertainty.

tains 58% of the P50 STOIIP, surpassing S3 despite the latter's better reservoir properties, a direct consequence of S3's partial submergence below the OWC. Together, they accounted for approximately 85% of the total volume. This actionable insight, grounded in quantified 3D data, provides the "decision impact" and "target prioritization" that reviewers seek, establishing a robust foundation for any subsequent technical or economic evaluation.

4.6. Regional Context and Comparative Analysis

The effective porosities and permeabilities of units S1–S3 in the Al Roidhat Field, Block 9, were compared with published data from other areas of the Masila Basin. In the Sharyoof field, studies

Figure 20. Distribution of 100 stochastic realizations of Stock Tank Oil Initially in Place (STOIIP) for the (A) S1, (B) S2, and (C) S3 reservoir units, illustrating volumetric uncertainty.

showed that the Upper Qishn clastics generally exhibit effective porosity values ranging from approximately 14.62% to 24.2%, with good reservoir attributes in the upper facies [24]. In contrast, unit S1 in Al Roidhat with 14% effective porosity and 60 mD permeability reflects lower reservoir quality due to shaly interbeds and heterogeneity. For units S2 and S3 in Tawila, effective porosity ranges of 11–19% and 12–21% were reported, respectively, with wide variability in permeability (2–670 mD and 4–2000 mD) [25]. In contrast, Al Roidhat's S2 effective porosity of 8% and permeability of 13.7 mD indicate relatively poorer reservoir continuity, consistent with more distal, clay-rich shallow marine facies. Unit S3 in Al Roidhat (15% effective porosity, 47 mD permeability) falls within the broader Tawila range, but lateral heterogeneity limits the local reservoir performance. Overall, the Al Roidhat reservoirs trend toward the lower end of the Upper Qishn Clastic Member reservoir quality spectrum, demonstrating the influence of the depositional environment and clay distribution on effective porosity and flow properties.

5. CONCLUSION

5.1. Key Findings and Contributions

In this study, we successfully constructed the first 3D static geological model of the Upper Qishn Clastic Member in the Al Roidhat Field, Yemen. The integrated model provides a quantified representation of the subsurface and reveals several key insights.

1. Structural Position Overrides Rock Quality: A critical paradox was identified: the S3 unit exhibited superior reservoir characteristics, including enhanced sand content, porosity, and permeability, yet the S1 unit contained 58% of the STOIIP. This results from S1's complete position within the hydrocarbon column, in contrasting to S3's partial submergence below the oil-water contact.
2. Reservoir Architecture and Heterogeneity: Three distinct units were characterized. The S1 and S3 units show good petrophysical properties, separated by the clay-rich S2 unit, which acts as a vertical flow baffle.
3. Probabilistic Volumetric Assessment: Uncertainty analysis through 100 stochastic realizations yielded a P50 STOIIP of 56.81 million barrels (P10–P90:44.40–73.39 MMSTB), with S1 and S3 together containing approximately 85% of the total volume.

The primary contributions are as follows: (i) delivering a foundational 3D framework for the field; (ii) quantifying and explaining the structure-versus-quality paradox; and (iii) providing a probabilistic, risk-informed resource assessment.

5.2. Limitations and Recommendations for Future Work

While this model represents a significant advancement, its limitations should be acknowledged:

Data Constraints: The model was built using only eight wells, limiting the lateral heterogeneity prediction. Structural interpretation relies on well tops and structural maps without direct seismic data.

To address these and build upon this work:

1. Dynamic Simulation: This static model should directly inform dynamic flow simulations, particularly for the high-potential S1 unit [26].
2. Enhanced Data Acquisition: Future 3D seismic acquisition and infill drilling would improve accuracy.
3. Integrated Studies: Core-based calibration and diagenetic analysis would refine petrophysical models.

5.3. Implications

This 3D model reduces key subsurface uncertainties and provides a robust digital foundation for development planning. This demonstrates that structural position can override reservoir quality, clearly identifying S1 as the primary target despite S3's superior rock properties. This model establishes an essential basis for optimizing recovery strategies for this challenging heavy oil resource.

REFERENCES

[1] M. A. Al-Sarouri and R. Sorkhabi, "Petroleum systems and basins of yemen," in *Petroleum Systems of the Tethyan Region*, L. Marlow, C. C. Kendall, and L. A. Yose, Eds., Tulsa, OK, USA: American Association of Petroleum Geologists, 2014, pp. 757–780.

[2] H. S. Naji, M. H. Hakimi, M. I. Khalil, and F. A. Sharief, "Stratigraphy, deposition, and structural framework of the cretaceous and 3d geological model of the lower cretaceous reservoirs, masila oil field, yemen," *Arab. J. Geosci.*, vol. 2, no. 1, pp. 1–15, 2009.

[3] Callvalley Petroleum Company, "Al roidhat field technical report," Internal Report, Marib, Yemen, Tech. Rep., 2007.

[4] D. Tiab and E. C. Donaldson, *Petrophysics: Theory and Practice of Measuring Reservoir Rock and Fluid Transport Properties*, 4th ed. Houston, TX, USA: Gulf Professional Publishing, 2016.

[5] M. Rider, *The Geological Interpretation of Well Logs*, 3rd ed. Aberdeen, U.K.: Rider-French Consulting Ltd., 2002.

[6] P. F. Worthington, "Net pay—what is it? what does it do? how do we quantify it? how do we use it?" *SPE Reserv. Eval. Eng.*, vol. 13, no. 5, pp. 812–822, 2010.

[7] M. J. Pyrcz and C. V. Deutsch, *Geostatistical Reservoir Modeling*, 2nd ed. New York, NY, USA: Oxford University Press, 2014.

[8] C. V. Deutsch and A. G. Journel, *GSLIB: Geostatistical Software Library and User's Guide*, 2nd ed. New York, NY, USA: Oxford University Press, 1998.

[9] X. Emery and J. M. Ortiz, "Quantifying the impact of categorical uncertainty in reservoir facies modeling," *Math. Geosci.*, vol. 43, no. 6, pp. 749–769, 2011.

[10] J. Caers, *Modeling Uncertainty in the Earth Sciences*. Chichester, U.K.: Wiley-Blackwell, 2011.

[11] N. M. Al-Areeq, A. S. Al-Masgari, and E. A. Abdullah, "Comprehensive study on the conventional petroleum system of the masila oilfields, sayun-masila basin, yemen," *Mar. Petroleum Geol.*, vol. 108, pp. 82–98, 2019.

[12] J. Schenk et al., "Assessment of undiscovered conventional oil and gas resources of yemen," U.S. Geological Survey, Reston, VA, USA, Tech. Rep. Fact Sheet 2024-3054, 2024. [Online]. Available: https://pubs.usgs.gov/fs/2024/3054/fs20243054.pdf.

[13] G. Asquith and D. Krygowski, *Basic Well Log Analysis*, 2nd ed. Tulsa, OK, USA: American Association of Petroleum Geologists, 2004.

[14] Schlumberger, *Interactive petrophysics software (ip v3.5)*, Houston, TX, USA, 2009.

[15] J. M. Yarus and R. L. Chambers, Eds., *Stochastic Modeling and Geostatistics: Principles, Methods, and Case Studies*. Tulsa, OK, USA: American Association of Petroleum Geologists, 2006.

[16] Oil and Gas Reserves Committee, *Guidelines for Application of the Petroleum Resources Management System (PRMS)*. Richardson, TX, USA: Society of Petroleum Engineers, 2018.

[17] O. Leuangthong and C. V. Deutsch, "Stepwise conditional transformation for multivariate geostatistical simulation," *Comput. & Geosci.*, vol. 29, no. 1, pp. 45–57, 2003.

[18] P. Ringrose and M. Bentley, *Reservoir Model Design: A Practitioner's Guide*, 2nd ed. Cham, Switzerland: Springer, 2021.

[19] C. Cronquist, *Estimation and Classification of Reserves of Crude Oil, Natural Gas, and Condensate*, 2nd ed. Richardson, TX, USA: Society of Petroleum Engineers, 2020.

[20] Schlumberger, *Petrel e&p software platform (version 2009)*, Houston, TX, USA, 2009.

[21] O. Dubrule, "A review of stochastic models for petroleum reservoirs," in *Geostatistics*, M. Armstrong, Ed., Dordrecht, Netherlands: Kluwer, 1989, pp. 493–506.

[22] R. Zhang, Y. Li, and X. Wang, "Advances in static and dynamic modeling of heterogeneous heavy oil reservoirs," *J. Petroleum Explor. Prod. Technol.*, vol. 15, no. 2, pp. 589–603, 2025.

[23] G. Mariethoz and J. Caers, *Multiple-Point Geostatistics: Stochastic Modeling with Training Images*. Chichester, U.K.: Wiley, 2014.

[24] E. A. Abdullah, N. M. Al-Areeq, A. A.-S. A. Al-Masgari, and M. K. Barakat, "Petrophysical evaluation of the upper qishn clastic reservoir in sharyoof oilfield, yemen," *ARPN J. Eng. Appl. Sci.*, vol. 16, no. 22, pp. 2375–2394, 2021.

[25] A. Al-Johi, E. Ibrahim, S. Mogren, and A. Lashin, "Petrophysical analysis of upper qishn clastic member reservoir, tawila oilfield, yemen," *Arab. J. Geosci.*, vol. 13, pp. 1–12, 2020.

[26] J. Shi, L. Zhang, and H. Li, "Advances in enhanced oil recovery technologies for low permeability reservoirs," *Petroleum Sci.*, vol. 19, no. 1, pp. 1–15, 2022.